

CHEMISTRY

A European Journal

A Journal of



Accepted Article

Title: Role of the bridging group in bis-pyridyl ligands: enhancing both photo- and electro-luminescent features of cationic (IPr)Cu(I) complexes

Authors: Margaux Elie, Michael D. weber, Florent Di Meo, fabien sguerra, Jean-François Lohier, Robert B. Pansu, Jean-Luc Renaud, Matthieu Hamel, Mathieu Linares, Rubén D. Costa, and Sylvain Gaillard

This manuscript has been accepted after peer review and appears as an Accepted Article online prior to editing, proofing, and formal publication of the final Version of Record (VoR). This work is currently citable by using the Digital Object Identifier (DOI) given below. The VoR will be published online in Early View as soon as possible and may be different to this Accepted Article as a result of editing. Readers should obtain the VoR from the journal website shown below when it is published to ensure accuracy of information. The authors are responsible for the content of this Accepted Article.

To be cited as: *Chem. Eur. J.* 10.1002/chem.201703270

Link to VoR: <http://dx.doi.org/10.1002/chem.201703270>

Supported by
ACES

WILEY-VCH

FULL PAPER

Role of the bridging group in bis-pyridyl ligands: enhancing both photo- and electro-luminescent features of cationic (IPr)Cu(I) complexes

M. Elie,^{[a]†} M. D. Weber,^{[b]†} F. Di Meo,^{[c],[d]†} F. Sguerra,^[e] J.-F. Lohier,^[a] R. B. Pansu,^[f] J.-L. Renaud,^[a] M. Hamel,^[e] M. Linares,^{*,[d],[g]} R. D. Costa,^{*,[b],[h]} S. Gaillard^{*,[a]}

Abstract: We report on the benefits of changing the bridging group X of bis-pyridyl ligands – *i.e.*, Py-X-Py where X is NH, CH₂, C(CH₃)₂ and PPh – on the photo- and electro-luminescent properties of a new family of luminescent cationic NHC copper(I) complexes (NHC : *N*-Heterocyclic Carbene). A joint experimental and theoretical study demonstrates that the bridging group rules the molecular conformation from a planar-like structure (X is NH and CH₂) to a boat-like structure (X is C(CH₃)₂ and PPh), leading to i) 4-fold enhancement of the photoluminescence quantum yield (ϕ_{em}) without affecting the thermally activated delayed fluorescence mechanism, and ii) one order of magnitude reduction of the ionic conductivity (σ) of thin films. This leads to an overall enhancement of the device efficacy and luminance due to the increased ϕ_{em} and the use of low applied driving currents.

Introduction

Significant attention has recently been devoted to the development of new organic or organometallic emitting emitters

for solid-state lighting technologies. In this field, a leading example is light-emitting electrochemical cells (LECs) due to its simpler architecture compared to organic light-emitting diodes (OLEDs).^[1] Indeed, the presence of ions in the active layer makes the use of charge transport and injection layers unnecessary. Up to now, one of the most successful families of LEC are those with active layers based on ionic transition noble metal complexes, such as iridium(III) and/or ruthenium(II). Despite the excellent device performance with respect to stability and efficiency, these types of emitters rely on rare metals, whose resources are not sustainable for a large-scale device production. Consequently, researchers have turned their attention to less expensive transition metal complexes, with copper(I) as a frontrunner.^[2] One of the assets of using copper(I) complexes^[3] is their unique emission mechanism based on a singlet harvesting process *via* thermally activated delayed fluorescence (TADF).^[4] Since the pioneering work of McMillin,^[5] many homoleptic and heteroleptic complexes with two bidentate diimine and diphosphine ligands have been studied. The main drawback of this family is the flattening process in the excited state that promotes an efficient ligand exchange.^[6-7] To circumvent this issue, a few new families of copper(I) complexes have recently emerged, namely i) cationic dinuclear copper(I) complex bearing tripodal phosphine and 4,4'-bipyridine bridging ligand,^[8] ii) cationic copper(I) with tripodal based pyridine and monophosphine ligands,^[9] and iii) cationic dinuclear copper(I) complexes bearing 3-(2'-pyridyl)pyrazole ligand and two diphosphine ligands bridging the two metal centers.^[10] Recently, *N*-Heterocyclic Carbenes (NHCs), which are known as a bulky and metal stabilizing ligands,^[11] have been envisaged for the development of new luminescent cationic copper(I) complexes.^[12] Among these cationic NHC copper(I) complexes, we^[13] and others^[14] have reported cationic three-coordinated copper(I) complexes, in which the "N²N ligand" was a 6-membered ring chelate with two pyridine rings and a borate^[14] or an amine^[13] as bridging group. In our previous studies, we reported a blue-emitting [Cu(IPr)(dpa)][PF₆] complex **1** (IPr = 1,3-bis(2,6-diisopropylphenyl)imidazol-2-ylidene, and dpa = di(2-pyridyl)amine)^[13a] and its application in LECs.^[13c] Here, we have identified key-structural and electronic parameters that clearly rule the photoluminescence features of this novel family of compounds. In few words, the dpa ligand leads to a non-coplanar geometry between the diamine ligand and the imidazole ring of the NHC.^[13a] The photoluminescence properties can also be modified by attaching electron donating and/or accepting groups at the periphery of the dpa ligand.^[13c]

- [a] M. Elie, J.-L. Lohier, Prof. J.-L. Renaud, Dr. S. Gaillard
Normandie Univ., LCMT, ENSICAEN, UNICAEN, CNRS, 14000, Caen (France).
sylvain.gaillard@ensicaen.fr
- [b] M. D. Weber, Dr. R. D. Costa
Department of Chemistry and Pharmacy, University of Erlangen-Nuremberg, Egerlandstr. 3, DE-91058 Erlangen (Germany).
- [c] Dr. F. Di Meo
INSERM UMR 850, Univ. Limoges, Faculty of Pharmacy, 2 rue du Dr. Marcland, F-87025 Limoges (France)
- [d] Dr. M. Linares
Division of Theoretical Chemistry and Biology, School of Biotechnology, KTH Royal Institute of Technology, SE-106 91 Stockholm (Sweden)
linares@kth.se
- [e] Dr. F. Sguerra, Dr. M. Hamel
CEA, LIST, Laboratoire Capteurs et Architectures Électroniques, F-91191 Gif-sur-Yvette Cedex (France).
- [f] Dr. R. B. Pansu
PPSM, CNRS, UMR8531 & Inst. d'Alembert FR3242, ENS Cachan, Paris Saclay University (France)
- [g] Dr. M. Linares
Swedish e-Science Research Centre, KTH Royal Institute of Technology, SE-104 50 Stockholm, (Sweden).
- [h] Dr. R. D. Costa
IMDEA Materials, C/ Eric Kandel, 2, Tecogetafe, 28906, Getafe, (Madrid)
ruben.costa@imdea.org
- Supporting information for this article is given via a link at the end of the document.

FULL PAPER

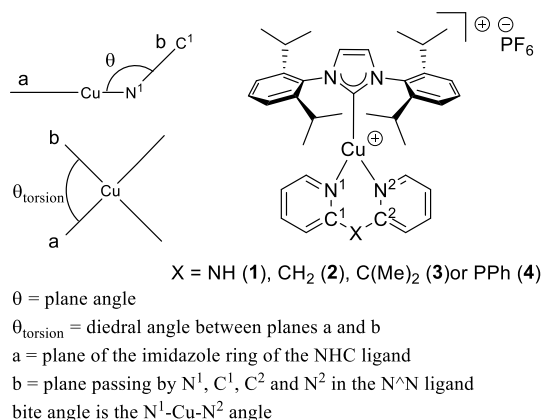


Figure 1. Definition of the plane angle θ and the torsion angle θ_{torsion} .

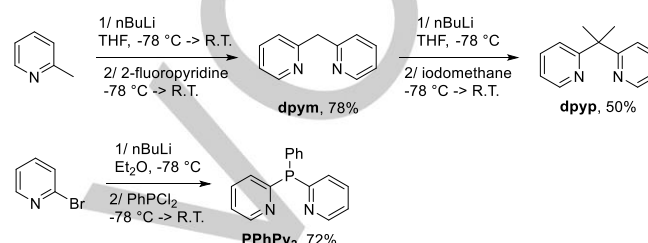
Indeed, the excellent photoluminescence features of NHC copper(I) complexes compared to those derived from McMillin works seems to be related to a significant breaking of the molecular symmetry towards an extended Y-shape geometry,^[16] compared to the tetrahedral one. Thanks to the 2,2'-bis-pyridyl derivatives which are six-membered chelate compared to the most encountered five-membered ring chelate ligands, such as 1,10-phenanthroline (phen) or 2,2'-bipyridine (bipy).^[13a] Unfortunately, LECs based on the archetypal complex **1** poorly performed – *i.e.*, luminance of 6 cd/m^2 and efficacy of 0.004 cd/A – due to the need of high applied currents (50 mA).^[13c] This scenario changed for devices with an emitter bearing a modified version of the dpa ligand – *i.e.*, luminance of 20 cd/m^2 and efficacy of 0.22 cd/A at applied currents of 5 mA.^[13c]

To further provide insights on how changing the molecular structure rules both the photo- and electro-luminescent features of NHC copper(I) complexes, we decided to study the role of the bridging atom. Our working hypothesis is to significantly force the molecular distortion of the dpa ligand *via* bridging atoms that lead to a tetrahedral conformation of this ligand. This should promote a significant symmetry breaking, leading to enhanced photoluminescence features and, in turn, better device performance should arise.

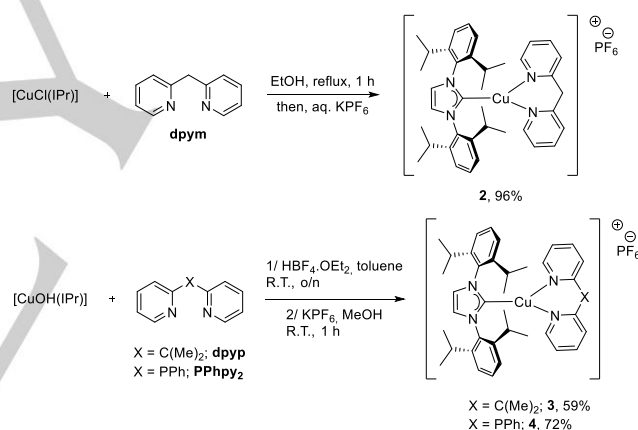
As such, this work describes the synthesis of a new series of cationic NHC copper(I) complexes coordinated to bis-pyridyl ligands (Fig. 1), having different bridging groups, such as NH (**1**), CH_2 (**2**), $\text{C}(\text{CH}_3)_2$ (**3**), or PPh (**4**). A joint experimental and theoretical study sheds light onto how structural and electronic changes related to the central atom of the bis-pyridyl ligand promote a more relevant symmetry break significantly affecting the maximum wavelength, the photoluminescence quantum yields (ϕ_{em}) and keeping the TADF emission mechanism. Finally, we also identified how the molecular changes affect the ionic conductivity (σ) of thin films, ruling the charge injection process under device operation conditions. Herein, a significant enhancement of the device luminance and efficacy reaching values of around 15 cd/m^2 and 0.4 cd/A are reported by replacing the NH bridging atom of the archetypal complex **1** for the novel PPh bridging atom of **4**.

Results and Discussion

Synthesis. The 2,2'-dipyridylmethane (dpym) ligand was prepared *via* $\text{S}_{\text{N}}\text{Ar}$ reaction between α -picolin and 2-fluoropyridine in 78% yield (Scheme 1).^[16] Dialkylation of dpym with iodomethane gave 2,2-(2,2'-dipyridyl)propane (dpyp) in 50% yield (Scheme 1).^[17] Finally, 2-bromopyridine was subjected to halogen/lithium exchange reaction and then engaged with dichlorophenylphosphine to furnish phenyl-2,2'-dipyridylphosphine (PPhpy₂) in 72% isolated yield (Scheme 1).^[18]



Scheme 1. Synthesis of N^N ligands with different bridging atoms.



Scheme 2. Synthesis of complexes **2-4**.

Complex **2** was prepared according to our previously reported procedure using $[\text{CuCl}(\text{IPr})]$ in 96% isolated yield (Scheme 2).^[13] For complexes **3** and **4**, the procedure using $[\text{CuCl}(\text{IPr})]$ failed to provide pure complexes. Therefore, complexes **3** and **4** were synthesized adding dpyp or PPhpy₂ ligands to $[\text{CuOH}(\text{IPr})]$ in the presence of one equivalent of $\text{HBF}_4\cdot\text{OEt}_2$, followed by an anion metathesis using KPF_6 in methanol. Complexes **3** and **4** were obtained in 59% and 72% overall yield, respectively (Scheme 2).^[13a,c]

Molecular and electronic structure study. To unambiguously establish the significance of the bridging atom on the molecular structure, single crystals were obtained and subjected to X-ray

FULL PAPER

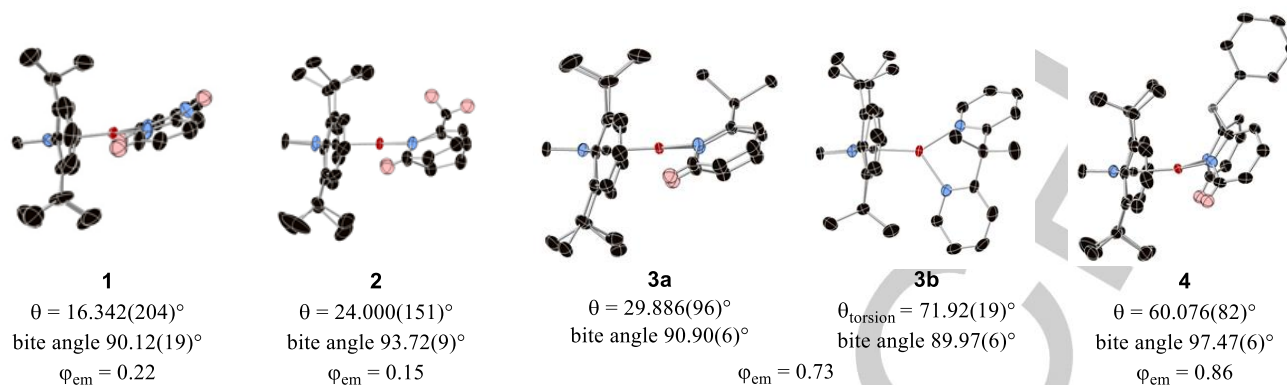


Figure 2. Ellipsoid representation of complexes **1-4** (lateral view exposing the plane angle Θ (Fig.1). The hydrogen atoms, the anions, and the numbering have been omitted for clarity. $\theta_{torsion}$ is the torsion angle between planes a and b (Fig.1). Please refer to Fig. S1 in the ESI for a top view of the three coordinated copper(I) metal center.

Table 1. Selected bond lengths and angles of complexes **1-4**.

Entry	Complex	Cu...C _{IPr} (Å)	Cu...N (Å)	N ¹ ...Cu...N ² (°)	N ¹ -C ¹ ...X-C ² (°)	Plane angle $\Theta^{[a]}$ (°)	CH...Cg ^[b] (Å)
1	1	1.918(4)	2.040(4) 2.065(4)	90.12(19)	19.896(370)	16.342(204)	2.56 2.42
2	2	1.906(2)	2.058(2) 2.063(2)	93.72(9)	57.352(229)	24.000(151)	2.58 2.62
3	3a	1.8985(16)	1.9859(14) 2.0495(14)	90.90(6)	63.48(18)	29.886(96)	2.66 2.61
4	3b	1.8767(16)	2.0415(14) 2.0455(14)	89.97(6)	61.38(20)	-	none
5	4	1.8935(17)	2.0169(15) 2.0617(14)	97.47(6)	63.059(103)	60.076(82)	none

^[a] The plane angle Θ is defined in Fig. 1. ^[b] Only CH- π interactions between the aromatic rings of IPr and the hydrogen atoms in alpha position of the bridged dipyrrolyl derivative were indicated.

diffraction (XRD). Fig. 1 defines some geometrical parameters, while Fig. 2 displays an ellipsoid representation of the molecular structures of **1**, **2**, **3a** and **3b** (where **3a** features the usual coordination of the N⁴N ligand and **3b** shows a twisted coordination of the N⁴N ligand), and **4**. In addition, the latter are provided along with a selection of the most relevant molecular structural parameters and photophysical properties (*vide infra*). In detail, a meaningful geometrical element is the plane angle Θ between the two ligands in the copper(I) complexes previously observed as defined in [Cu(NHC)(dpa)][X] (Fig. 1).^[13c] Another key parameter is the torsion angle $\Theta_{torsion}$ between the two ligands. This was previously defined by Thompson and Yersin for NHC copper(I) complexes coordinated to dimethyldipyrrolylborate ligand.^[14b] A direct comparison of those XRD analyses allows to highlight four relationships between the structure and the chemical nature of the ligands. Firstly, the expected 6-membered-ring coordination of both ligands in **2**, **3a**, **3b**, and **4** was confirmed (Fig. 2 and Fig. S1), even though PPhpy₂ ancillary ligand could also promote a competitive coordination with the bridging phosphorus atom.^[19] Secondly, the three new ligands dpym, dpyp and PPhpy₂ have adopted a boat-like conformation in regards

with the six-membered ring, including the Cu(I) metal center (Fig. 2). This leads to higher distorted conformations compared to the dpa ligand in **1** (Fig. 2). This is illustrated by the values of the N¹-C¹...X-C² dihedral angles: 19.9(4), 57.4(2), 63.5(2) and 63.1(1)° of complexes **1**, **2**, **3a**, and **4**, respectively (Table 1). The boat conformation is caused by a more pronounced pyramidal geometry of the carbon and phosphorus bridging atoms. Noteworthy, the dihedral angle in dpym in **2** is increased by around 6° compared to that noted in dpym in **2** due to the presence of the *gem*-dimethyl substituent generating tetrahedral distortion by their steric hindrances and electronic repulsion, the so-called Thorpe-Ingold effect, while it is close to the one in PPhpy₂ (**4**).^[20] Another important geometry modification concerned the plane angles Θ (Fig. 1) in complex **4** with a value found at 60.1(1)°. Θ values were found at 16.3(2), 24.0(2) and 29.9(1)° in **1**, **2**, and **3a**, respectively (Table 1). From a structural point of view, the high Θ value in **4** leads to the loss of the CH- π interactions that are usually observed between the aromatic rings of IPr and the hydrogen atoms of the bis-pyridyl derivatives. Such substantial increase of the Θ value is correlated with the Cu-C_{IPr} bond lengths,

FULL PAPER

which diminish from 1.918(4), 1.906(2), 1.899(2) and 1.894(2) Å in **1**, **2**, **3a**, and **4**, respectively (Table 1).

The last observation came from the variation of the bite angle, which increases from 90.1(2), to 90.9(1), to 93.7(1), and to 97.5(1)° for **1**, **3a**, **2**, and **4**, respectively (Table 1). Again, the Thorpe-Ingold effect might explain the value of the bite angle in **3a**. This is lower than the one in **2**, but closer to that in **1** (90.1(2) vs. 90.9(1)°, Table 1).

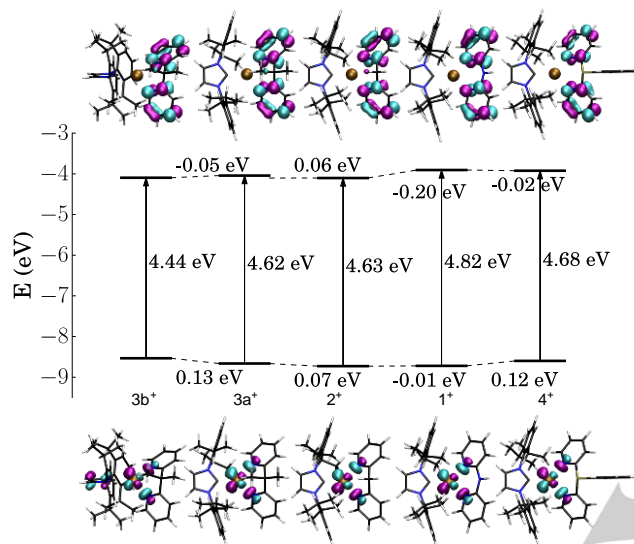


Figure 3. HOMO and LUMO distributions and energies as well as HOMO-LUMO gaps for complexes [Cu(IPr)(dpa)]⁺ (**1***), [Cu(IPr)(dpym)]⁺ (**2***), [Cu(IPr)(dppp)]⁺ (**3a*** and **3b***) and [Cu(IPr)(PPhPy₂)]⁺ (**4***) (isovalues: 0.005 e.a₀⁻³, [Cu(IPr)(dpa)]⁺ (**1***) is taken as initial reference).

Next, changes of the electronic structure of this family of complexes were investigated via density functional theory (DFT) calculations. Here, the models [Cu(IPr)(dpym)]⁺ (**2***), [Cu(IPr)(dppp)]⁺ (**3a*** and **3b***) corresponding to the two conformers observed by XRD analysis) and [Cu(IPr)(PPhPy₂)]⁺ (**4***) were compared to the archetypal [Cu(IPr)(dpa)]⁺ (**1***) (Fig. 3). Common to all complexes, the HOMO is located at the Cu-atom 3d and N_{pyridyl} 2p_z orbitals, while the LUMO is centered on both pyridine rings (Fig. 3), suggesting a strong ground state charge transfer (GS-CT) nature. Electron population analysis highlights,

however, a weaker GS-CT in fully π -conjugated ligands – i.e., **1*** and **4*** with respect to **3*** and **2*** (see ESI, Table S6). The decrease of π -conjugation in bis-pyridyl ligand leads to an electron enrichment in N-Cu-(N⁺N) region and a HOMO destabilization. Noteworthy, the absence of a π -conjugation between pyridyl moieties increases the GS-CT from both NHC and bis-pyridyl ligand. This is associated to an increase of the electron population that strongly stabilizes the LUMO. Even though electronic effects are different, **2***, **3***, and **4*** exhibit lower HOMO-LUMO gaps than that of **1***, owing to a lower π -conjugation within only the bis-pyridyl moiety. On one hand, **2*** and **3*** feature a broken π -conjugation due to the bridging carbon atom. On the other hand, **4*** shows a decreased bis-pyridyl π -conjugation due to the presence of an attractive phenyl moiety and the more pyramidal geometry of the phosphorus bridging atom. Hence, these findings confirm that our approach was successful with respect to the expected molecular distortions provided by the nature of the bridging atom.

Photophysical study. The absorption spectra of **2**, **3**, and **4** show a first intense band assigned to a π - π^* transition of the ancillary ligands between 244 and 269 nm with an additional band at 279 nm in the case of **4** (Table 2). More interesting are the shifts related to the d- π^* metal-to-ligand charge transfer (MLCT) absorption bands, which are typically influenced by changes in the molecular structure. For instance, a red-shifted (10 nm) MLCT band was observed for **1** and **2** compared to that of **3**, while a more significant red-shift of around 15 nm was noted for **4** (25 nm if **3** is considered as a reference). This trend could be explained by the changes of the electron donation character related to the central atom. For instance, the lone pair of the nitrogen bridging atom is involved in the π -conjugation within both pyridine rings (*vide supra*), while the geometry of the phosphorus bridging atom implies that inductive effects are more important than mesomeric effects, leading to a strong electron-withdrawing character. As the methylene groups in dpym and dppp ligands feature an electron-donor character caused by inductive effects, central atoms in the different ligands appear to be ranged for these electronic donation as follow: nitrogen, carbon and phosphorus. This is in line with our previous observation in [Cu(IPr)(dpa)][PF₆] derivatives, in which the more electron rich the dpa, the more blue-shifted the emission wavelength peak.^[13c]

Table 2. Photoluminescence data of **1-4**.

Entry	Complex ^[a]	Absorption ^[a]	Emission ^[d]							
		λ_{max} [nm]	λ_{em} [nm] at 298 K ^[e]	λ_{em} [nm] at 77 K	$\Delta\lambda_{\text{em}}$ [eV]	Φ_{em} ^[e]	τ_{em} [μs] at 298 K	τ_{em} [μs] at 77 K	k_r [10 ⁴ s ⁻¹] at 298 K	k_{nr} [10 ⁴ s ⁻¹] at 298 K
1	1	260 (2.31), 315 (1.37) ^[b]	463	481	0.10	0.22	13	45	1.7	6.0
2	2	269 (1.34), 315 (0.27) ^[c]	473	483	0.12	0.15	6	32	2.5	14.2
3	3	265 (1.30), 305 (0.30) ^[c]	474	482	0.10	0.73	14	38	5.2	1.9
4	4	244 (1.77), 279 (1.46), 330 (0.44) ^[c]	503	519	0.10	0.86	13	87	6.6	1.1

FULL PAPER

[a] In brackets ϵ [$10^4 \text{ L}\cdot\text{mol}^{-1}\cdot\text{cm}^{-1}$]. [b] In CHCl_3 solution. [c] In CH_2Cl_2 solution. [d] Powder. [e] Error of 0.05.

Table 3. Calculated vertical transition energies (E), absorption wavelength (λ) and corresponding main MO description for each band.

Complex	Band	E (eV)	λ (nm)	main MO contribution	Type
$[\text{Cu}(\text{lpr})(\text{dpa})]^+ (\mathbf{1}^+)$	I	4.26	291.3	H-2 \rightarrow L(58%)	MLCT/IL(π - π^*)
		4.36	284.3	H-2 \rightarrow L+1(73%)	MLCT/IL(π - π^*)
	II	4.99	248.4	H-2 \rightarrow L+2(72%)	MLCT/IL(π - π^*)
$[\text{Cu}(\text{lpr})(\text{dpym})]^+ (\mathbf{2}^+)$	I	3.72	333.2	H-1 \rightarrow L (93%)	MLCT
	II	4.32	286.9	H-2 \rightarrow L (69%)	(ML/NHC)-CT
$[\text{Cu}(\text{lpr})(\text{dpy})]^+ (\mathbf{3a}^+)$	I	3.80	326.3	H-1 \rightarrow L(93%)	MLCT
	II	4.36	284.5	H-2 \rightarrow L(59%)	(ML/NHC)-CT
$[\text{Cu}(\text{lpr})(\text{dpy})]^+ (\mathbf{3b}^+)$	I	3.87	320.7	H-1 \rightarrow L(96%)	MLCT
	II	4.49	276.2	Complex	(ML/NHC)-CT
$[\text{Cu}(\text{lpr})(\text{PPhpy}_2)]^+ (\mathbf{4}^+)$	I	3.80	326.5	H-1 \rightarrow L (88%)	MLCT
	II	4.34	285.6	H-2 \rightarrow L(81%)	IL(ν/π - π^*)
		4.39	282.2	H-3 \rightarrow L(51%)	NHC-CT
	III	5.13	241.9	H-2 \rightarrow L+4(63%)	IL(ν/π - π^*)

To further confirm these notes, the adiabatic $S_0 \rightarrow S_x$ vertical transitions were calculated within the Time-Dependent DFT (TD-DFT) framework (see ESI, Fig. S11-S15). Such approach enables to describe up to three main types of transitions, for which contributions are i) MLCT, ii) intraligand $\pi \rightarrow \pi^*$ transition, and iii) NHC to ligand charge transfer (NHC-CT) (Table 3). As a matter of fact, both the nature and the energy of the electronic transitions are strongly dependent on the bridging atom of the bis-pyridyl ligand. For instance, the low decrease of the band intensity assigned to the MLCT transition is noted for complexes with lower π -conjugation over the bis-pyridyl moiety (i.e., lower oscillator strength, see Fig. S11-S15). Based on the calculation on $\mathbf{2}^+$ and $\mathbf{3a}^+$ and $\mathbf{3b}^+$, the bands located at 265 and 269 nm for $\mathbf{2}$ and $\mathbf{3}$ are assigned to a mixture of MLCT and NHC-CT, respectively, and the bands at 315 and 305 nm are assigned to a pure MLCT. Interestingly, from the calculation achieved on $\mathbf{4}^+$, the band at 279 nm involves two distinct types of transition, i.e., IL($\pi \rightarrow \pi^*$) transition ($S_0 \rightarrow S_2$) and NHC-CT transition ($S_0 \rightarrow S_3$). The former is red-shifted with respect to $\mathbf{1}^+$ since the phenyl moiety increases the overall π -conjugation over the whole ligand (see ESI). The last band of $\mathbf{4}$ located at 244 nm is assigned to a pure IL($\pi \rightarrow \pi^*$)-type transition (see Fig. S12-S15).

Next, the impact of the bridging atom on the photoluminescence features of the complexes were investigated. All the complexes show a broad and featureless emission band, suggesting a charge transfer nature for the emitting excited state. In addition, the emission maximum is red-shifted for $\mathbf{2}$ (473 nm), $\mathbf{3}$ (474 nm), and $\mathbf{4}$ (503 nm) compared to that of $\mathbf{1}$ (463 nm) (Table 2). Interestingly, all the complexes show red-shifted emission at 77 K (Fig. 4 and Table 2), pointing out a TADF emission mechanism, as widely described in the literature.^[4] This was further confirmed measuring the excited state lifetime (τ_{em}) of the emission at 77 K. Indeed, all τ_{em} increased by a factor of at least 2.7 (minimum factor calculated for $\mathbf{3}$) going from room temperature to 77 K (Table 2). Such increase of τ_{em} resulted from a change in the nature of the emitting excited state from singlet to triplet. Then, the central substitution on the bis-pyridyl ligand and its ability to participate into the π -conjugation seems to not

significantly modify the $\Delta\lambda_{\text{em}}$ - i.e. the difference of energy between the singlet and the triplet excited states ruling the TADF process (Table 2). This parameter has been calculated by monitoring the changes of τ_{em} in function of the temperature (between 77 and 298 K), fitting them using the same TADF model previously used.^[13c,21]

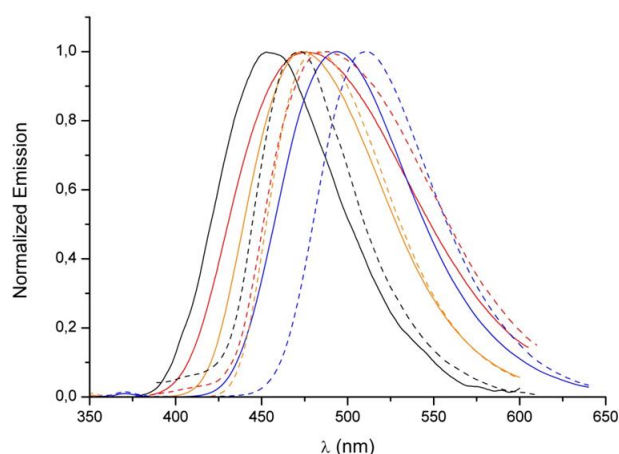


Figure 4. Photoluminescence spectra in solid state (powder) at room temperature (solid line) and at 77 K (dotted line) of complexes $\mathbf{1}$ (black), $\mathbf{2}$ (red), $\mathbf{3}$ (orange) and $\mathbf{4}$ (blue).

Considering the direct fluorescence lifetimes, they were calculated at 670, 9.4, 141 and 101 ns for $\mathbf{1}$, $\mathbf{2}$, $\mathbf{3}$ and $\mathbf{4}$, respectively. The phosphorescence lifetimes were estimated at 45, 19.6, 37.1 and 86 μs for $\mathbf{1}$, $\mathbf{2}$, $\mathbf{3}$ and $\mathbf{4}$, respectively. As such, the $\Delta\lambda_{\text{em}}$ values were calculated at 0.095, 0.12, 0.10, and 0.10 eV for complexes $\mathbf{1}$, $\mathbf{2}$, $\mathbf{3}$ and $\mathbf{4}$, respectively. (ESI, Fig. S7-S9 and Table S2-S4).

Theoretical calculations further support these findings. In short, S_1 and T_1 were optimized following the same approach as our

FULL PAPER

previous study,^[13c] but at the PBE0/6-31+G(d,p)/SDD level of theory. This functional has been chosen for its capability to accurately describe intramolecular CT.^[22] Estimated $\Delta\lambda_{\text{em}}$ values were in perfect agreement with those experimentally obtained (Tables 2 and 4). Likewise, calculated $S_1 \rightarrow S_0$ vertical energies that correspond to the fluorescence process were in good agreement with the experimental observation at 298 K, given the spectroscopic accuracy of TD-DFT calculations.

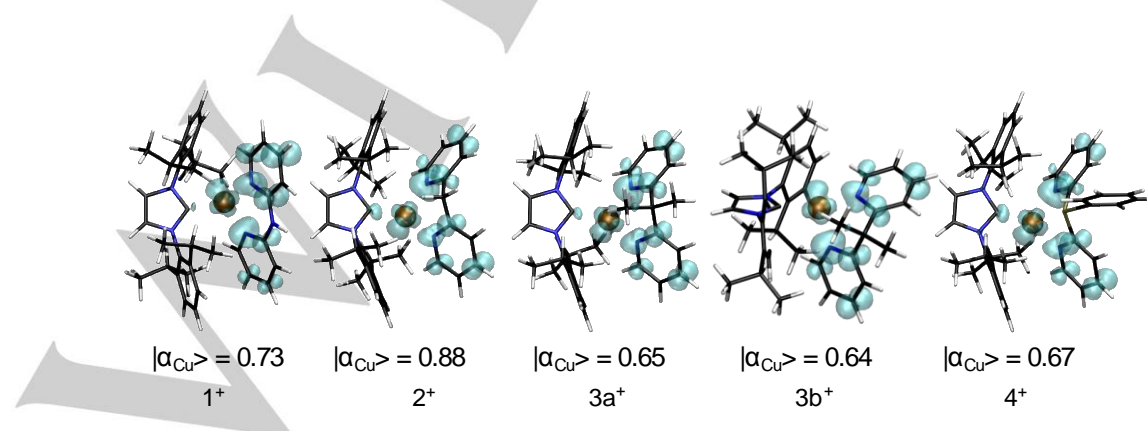
The rationalization of τ_{em} at 298 K is a challenging task, since it depends on collective properties, namely i) singlet-triplet energy splitting, ii) triplet state stability, and iii) geometrical deformations between T_1 and S_1 ; the lower the S_1/T_1 geometrical deformation, the faster the back-ISC process, and the lower the τ_{em} . Complexes exhibit singlet-triplet splitting in the same range which is in good agreement with experimental data (*i.e.*, ca. 0.10 eV, Table 4). The lower τ_{em} value of **2** might be explained by (i) a slightly less stable triplet state associated to a larger Cu-atom spin density ($|\alpha_{\text{Cu}}| = 0.88$ found for **2**⁺, see Fig. 5) and ii) a smaller deviation of both folding and rotation parameters between S_1 and T_1 geometries (see ESI, Fig. S17). In addition, the triplet stability improves by increasing π -conjugation ($|\alpha_{\text{Cu}}|$ being 0.73 and 0.67 in **1**⁺ and **4**⁺, respectively).

In agreement with our previous study, both the rotation of bis-pyridyl ligand with respect to $\text{C}_{\text{NHC}}\text{-Cu(I)}$ bond and the folding of the bis-pyridyl ligand (see ESI, Fig. S17) seems to play a key role in the kinetic of the back-ISC event. The presence of bulky moieties (*e.g.*, methyl or phenyl moieties respectively in **3** and **4**) is associated to i) a stronger deformation and ii) a lower flexibility of bis-pyridyl ligand that might explain a longer excited state lifetime values, suggesting a strong reduction of the non-radiative decay process.

Although, the bridging atom does not substantially affect the TADF emission mechanism in this family of compounds, there is a strong enhancement of the ϕ_{em} values upon comparing **1** and **2** with **3** and **4** (*i.e.*, 0.15, 0.22, 0.76, 0.86, respectively, Table 2). For instance, the addition of two methyl substituents at the bridging atom (**2** vs. **3**) leads to a more important symmetry breaking generated by a higher value of the plane angle Θ ($24.000(151)^\circ$ in **2** vs. $29.886(96)^\circ$ in **3a**), the more pronounced pyramidal geometry of the bridging atom ($57.352(229)^\circ$ in **2** vs. $63.48(18)^\circ$ in **3a**) and the presence of a the twisted conformer **3b** lead to enhanced photoluminescence ($\phi_{\text{em}} = 0.15$ for **2** vs. $\phi_{\text{em}} =$

0.73 for **3**). Following this rationale, a very high ϕ_{em} of 0.86 was measured for **4**. Here, the plane angle Θ and the pyramidal geometry of the phosphorus atom are more pronounced with respect to that of **3** (Fig. 2). Finally, **1**⁺ exhibits the strongest geometry deformation between both S_1 and T_1 state. The planarity related to the π -conjugation over the ligand decreases the flexibility of bridged bis-pyridyl derivatives dihedral angles. This results in an easier recombination from T_1 to S_1 excited states, since the ligand just has to rotate around $\text{C}_{\text{NHC}}\text{-Cu(I)}$ bond contrary to other complexes with more pyramidal bridging atom – *i.e.*, carbon or phosphorus atom. Flexibility is also likely involved for explaining the ϕ_{em} trends. The higher the flexibility, the lower the barrier for the non-radiative recombination to S_0 state, explaining the lower ϕ_{em} of **1** and **2**. Geometry-dependent TADF was assessed by calculating singlet-triplet splitting on both **3a**⁺ and **3b**⁺ conformers. The role of $\text{N}^1\text{-C}^1\text{...X-C}^2$ to TADF is still under debate, since it has been shown to decrease TADF occurrence in boron-based dpa ligand,^[14b] but not in bidentate phenanthroline one.^[23] Our findings agree with the latter, two conformations exhibiting similar singlet-triplet splitting (0.09 and 0.10 eV respectively for conformation a and b, Table 4). This confirms the importance of joint i) ligand flexibility and ii) S_1/T_1 geometry deformation rather than the orientation itself. The dpyp ligand can swap from T_1 to S_1 independently on its orientation contrary to neutral boron-based dpa ligand. To put it in a nutshell, our joint photophysical and theoretical study highlights that the replacement of the nitrogen atom by more pyramidal atom significantly enhances the radiative deactivation pathway from the singlet excited state without affecting the TADF mechanism.

Electroluminescent study. Having rationalized the impact of the bridging atom on the photoluminescence features, we turned to investigate the electroluminescence behavior in a simple two-layer LEC device. In short, a 90 nm active layer consisting on the copper(I) complexes was deposited onto a Indium-Tin oxide (ITO) electrode coated with a 70 nm PEDOT:PSS layer. To finalize the device, a 90 nm aluminum cathode was evaporated. In order to provide a direct comparison between complexes, the devices were tested using a driving scheme based on a pulsed-current block wave at 1 kHz and a duty cycle of 50% (see ESI, Fig. S18). As previously noted for LECs based on **1**,^[13c] the color stability is significantly compromised upon using high pulsed currents due to the prominent degradation of the emitter.



FULL PAPER

Figure 5. Triplet spin density plots of complexes [Cu(Ipr)(dpa)]⁺ (**2**⁺), [Cu(Ipr)(dpym)]⁺ (**3a**⁺), [Cu(Ipr)(dpyp)]⁺ (**3b**⁺) and [Cu(Ipr)(PPhpy₂)]⁺ (**4**⁺) (isovalues: 0.005 e.a₀⁻³).

Table 4. Calculated vertical S₁→S₀, T₁→S₀ emission energies (in eV). The theoretically estimated and experimental singlet-triplet energy splitting are also provided.

Complex	E _{vert} ^{S₁→S₀} (eV)	E _{vert} ^{T₁→S₀} (eV)	ΔE ^{S/T}	
			Theo. (eV)	Exp. (eV)
[Cu(Ipr)(dpa)] ⁺ (1 ⁺)	2.40	2.19	0.08	0.10
[Cu(Ipr)(dpym)] ⁺ (2 ⁺)	2.40	2.10	0.07	0.12
[Cu(Ipr)(dpyp)] ⁺ (3a ⁺)	2.45	2.14	0.09	0.10
[Cu(Ipr)(dpyp)] ⁺ (3b ⁺)	2.46	2.14	0.10	0.10
[Cu(Ipr)(PPhpy ₂)] ⁺ (4 ⁺)	2.34	2.09	0.06	0.10

However, high pulsed currents of around 50 mA are necessary to inject enough charges to reach a light output superior to 1 cd/m². This turns these devices very inefficient with an efficacy value of around 4 × 10⁻³ cd/A. In order to shed light onto the poor charge injection mechanism, we determined the ionic conductivity (σ) via electrochemical impedance spectroscopy technique (see experimental section). This parameter rules the formation of electrical double layers (EDLs) that assist charge injection in LECs.^[24] In detail, devices with **3** and **4** feature similar σ values of 8 × 10⁻⁸ and 6 × 10⁻⁸ S/m, respectively. Both values significantly contrast with that of devices with **2** (4 × 10⁻⁹ S/m), while the σ value of devices with **1** could not be determined with enough accuracy due to the high resistance value. Quite likely, the enhanced ionic mobility feature of **3** and **4** should be related to distorted geometry caused by the bridging atom that reduces the cation-ion binding energy (E_{c-a}). In other words, devices with **3** and **4** should easily form the EDLs, allowing to apply low currents, while **1** and **2** should not show any electroluminescence response. Both, σ and φ_{em} parameters, prompt to a significant enhancement of the device efficiency upon changing the bridging atom going from **1** and **2** to **3** and **4**.

To confirm this notion, all of the devices were driven at different pulsed currents going from 0.5 to 5 mA. At the lowest applied current – Fig. 6 and Table 5, devices with **3** and **4** feature an almost instantaneous electroluminescence response, achieving luminance and efficacy values up to 6.2 cd/m² and 0.19 cd/A and up to 13.0 cd/m² and 0.39 cd/A, respectively. As expected, devices with **1** and **2** did not show neither electrical response nor light output. The latter showed an electroluminescence behavior at applied currents of 5 mA, reaching luminance and efficacy values of around 2 cd/m² and 1 × 10⁻² cd/A, respectively – Table 5 and Fig. S18. Noteworthy, the luminance (30 cd/m²) and efficacy (0.15 cd/A) of devices with **4** hold upon using 5 mA pulsed currents – Table 5.

This significant improvement might be solely ascribed to the enhancement of both σ and φ_{em} upon only changing the bridging atom of the bis-pyridyl ligand. Indeed, under the above-mentioned driving conditions, devices show a similar mechanism as derived from the average voltage profile, that is, an immediately drop to a plateau due to the formation of the EDLs and a slow increase caused by the degradation of the active layer. As far as the decay

of the luminescence is concerned, this might be related to the quenching of the emission by the approaching of the p- and n-doped regions reducing the thickness of the emitting junction. Finally, changes in the EL spectrum were not noted under device operation conditions, showing a light blue (**1** and **2**), blue (**2**), greenish blue (**3**), and dark green (**4**) emission with x/y color coordinates of 0.23/0.28, 0.30/0.42, 0.23/0.39, and 0.31/0.51, respectively.

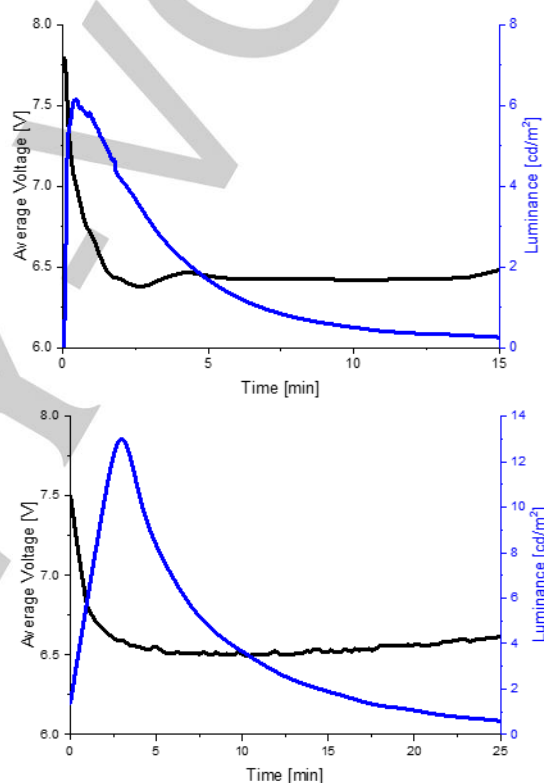


Figure 6. Luminance and average voltage vs. time of devices prepared with **3** (top) and **4** (bottom) driven at 0.5 mA pulsed mode with a block wave form at 1 kHz and a duty cycle of 50%.

Table 5. Figures-of-merit of devices prepared with **1-4** driven at different pulsed currents (I_{avg}).

Complex	Electroluminescence			
	I _{avg} [mA]	Lum. [cd/m ²] ^[a]	Efficacy [cd/A]	t _{1/2} [s] ^[b]
1	5	2.6	0.007	44
2	5	2.2	0.001	36
3	0.5	6.2	0.19	240
	5	21.5	0.067	324
	0.5	13	0.39	

FULL PAPER

4	5	32	0.10	42
				10

[a] Lum corresponds to the maximum luminance value. [b] $t_{1/2}$ is the time to reach half of the maximum luminance.

Conclusions

This work demonstrates, with the support of both experimental and theoretical studies, that the nature of the bridging atom between the two coordinating pyridine rings plays an important role on the photo- and electro-luminescent properties of NHC copper(I) complexes. Indeed, the molecular distortion is a key parameter to design new complexes for lighting applications. This work discloses that moving from a planar-like structure (X is NH (**1**) and CH₂ (**2**)) to a boat-like structure (X is C(CH₃)₂ (**3**) and PPh (**4**)) of the bis-pyridyl ligand significantly enhances the ϕ_{em} without affecting the TADF mechanism. In addition, this distortion strongly increases the σ of thin films, leading to the easy formation of EDLs under low applied currents. As such, devices with the new complexes **3** and **4** outperformed the current state-of-the-art in LECs based on NHC copper(I) complexes. Here, moderate luminance (10–15 cd/m²) and efficacy (0.2–0.4 cd/A) values were reached under applied low currents (0.5 mA). Noteworthy, these features hold upon increasing the applied currents up to 5 mA, outperforming devices prepared with the archetypal complex **1** luminance (3 cd/m²) and efficacy (7 × 10^{−3} cd/A). Overall, this work provides key information of how enhancing both photo- and electro-luminescent features of an emerging family of copper(I) complexes.

Experimental Section

General Considerations. All reactions were carried out using standard Schlenk technique under an atmosphere of dry Argon. Solvents were purchased from Carlo Erba and degassed prior to use by bubbling argon gas directly in the solvent. Solvents for NMR spectroscopy were dried over molecular sieves. NMR spectra were recorded on 400 MHz and 500 MHz Bruker spectrometers. Proton (¹H) NMR information is given in the following format: multiplicity (s, singlet; d, doublet; t, triplet; q, quartet; quintet; sextet; septet; m, multiplet), coupling constant(s) (*J*) in Hertz (Hz), number of protons. The prefix *app* is occasionally applied when the true signal multiplicity was unresolved and *br* indicates the signal in question is broadened. Carbon (¹³C) NMR spectra are reported in ppm (δ) relative to residual CHCl₃ (δ 77.0) unless noted otherwise and information on carbon multiplicity is given in the following format: multiplicity (s, singlet for C; d, doublet for CH; t, triplet for CH₂ and q, quartet for CH₃). The full signals attributions are given in ESI, as well as the copy of the NMR spectra. HRMS were performed by LCMT analytical services. NMR solvent was passed through a pad of basic alumina before uses. 2,2'-dipyridylamine was purchased from Sigma-Aldrich and used without prior purification. The copper complexes [CuCl(IPr)]^[25] and [CuOH(IPr)]^[26] were synthesized following reported procedures.

Complex 2. In a flame-dried Schlenk tube under an argon atmosphere, [CuCl(IPr)] complex (150 mg, 0.30 mmol) and ligand dpym (55 mg, 0.32

mmol) were dissolved in degassed absolute ethanol (7.5 mL) and heated under reflux for one hour. After cooling down the reaction mixture to room temperature, aqueous solution of KPF₆ (166 mg, 0.9 mmol in around 5 mL of water) was added affording a white precipitate. The solid was collected on a frit, washed with water and dried under air and then under vacuum. The copper complex [Cu(IPr)(dpym)][PF₆] (**2**) was obtained as a light brown powder (220 mg, 0.29 mmol, 96% yield). ¹H-NMR (CDCl₃, 400 MHz): 1.11 (d, *J* = 6.8 Hz, 12H), 1.23 (d, *J* = 6.8 Hz, 12H), 2.72 (sept, *J* = 6.8 Hz), 3.88 (s, 2H), 6.89–6.93 (m, 4H), 7.27–7.32 (m, 6H), 7.48–7.53 (m, 4H), 7.67 (dt, *J* = 1.6 and 7.6 Hz, 2H) ppm. ¹³C-NMR (CDCl₃, 100 MHz): 24.0 (qx4), 24.2 (qx4), 28.8 (dx4), 43.6 (t), 122.8 (dx2), 123.5 (dx2), 124.4 (dx4), 125.5 (dx2), 130.6 (dx2), 135.8 (sx2), 139.3 (dx2), 145.8 (sx4), 148.9 (dx2), 154.6 (sx2), 183.6 (s) ppm. IR (neat): ν 2965, 1600, 1573, 1471, 1443, 836 cm^{−1}. HRMS (ESI): *m/z* calcd for C₃₈H₄₆N₄Cu [M-PF₆]⁺: 621.3018; found: 621.3040.

Complex 3. In a flame-dried Schlenk tube under an argon atmosphere, [CuOH(IPr)] complex (234.6 mg, 0.5 mmol) and 2,2'-dipyridyl-2,2-propane (dpyp) (99.1 mg, 0.5 mmol) were dissolved in dry degassed toluene. HBF₄·Et₂O (68 μ L, 0.5 mmol) was added dropwise and the reaction mixture was stirred overnight at room temperature. Pentane was added, affording a white precipitate which was collected on a frit, washed with pentane and dried under vacuum. Then, in a round bottom flask, the [Cu(IPr)(dpyp)][BF₄] complex and KPF₆ (304 mg, 1.65 mmol) were dissolved in MeOH. The mixture was stirred for 1 hour at room temperature and then concentrated to dryness. The crude mixture was dissolved in dichloromethane, filtered through a pad of Celite® and concentrated under vacuum, leading to the pure copper complex [Cu(IPr)(dpyp)][PF₆] (**3**) as a white-yellowish powder (237 mg, 0.30 mmol, 59% yield). ¹H-NMR (CDCl₃, 400 MHz): 1.12 (d, *J* = 6.8 Hz, 12H), 1.24 (d, *J* = 6.8 Hz, 12H), 1.69 (s, 6H), 2.80 (sept, *J* = 6.8 Hz, 4H), 6.95 (m, 2H), 7.08 (d, *J* = 4.3 Hz, 2H), 7.32 (d, *J* = 7.6 Hz, 4H), 7.33 (s, 2H), 7.50–7.57 (m, 4H), 7.72 (t, *J* = 7.3 Hz, 2H) ppm. ¹³C-NMR (CDCl₃, 100 MHz): 23.5 (qx4), 24.9 (qx4), 28.7 (dx4), 44.5 (s), 121.6 (dx2), 122.6 (dx2), 123.9 (dx2), 124.4 (dx4), 130.7 (dx2), 135.8 (sx2), 139.3 (dx2), 145.9 (sx4), 149.5 (dx2), 161.6 (sx2), 183.2 (s) ppm. IR (neat) ν 1595, 1464, 1402, 1365, 1327, 1061, 838, 803, 761, 743 cm^{−1}. HRMS (ESI): *m/z* calcd for C₄₀H₅₀N₄Cu [M-PF₆]⁺: 649.3331; found: 649.3333.

Complex 4. In a flame-dried Schlenk tube under an argon atmosphere, [CuOH(IPr)] complex (155 mg, 0.33 mmol) and bis(2-pyridyl)phenylphosphine (PPhpy₂) (87 mg, 0.33 mmol) were dissolved in dry degassed toluene. HBF₄·Et₂O (45 μ L, 0.33 mmol) was added dropwise and the reaction mixture was stirred overnight at room temperature. Pentane was added, affording a white precipitate which was collected on a frit, washed with pentane and dried under vacuum. Then, in a round bottom flask, the [Cu(IPr)(PPhpy₂)] [BF₄] complex and KPF₆ (304 mg, 1.65 mmol) were dissolved in MeOH. The mixture was stirred for 1 hour at room temperature and then concentrated to dryness. The crude mixture was dissolved in dichloromethane, filtered through a pad of Celite® and concentrated under vacuum, leading to the pure copper complex [Cu(IPr)(PPhpy₂)] [PF₆] (**4**) as a yellowish powder (205 mg, 0.24 mmol, 72% yield). ¹H-NMR (CDCl₃, 400 MHz): 1.16 (d, *J* = 6.9 Hz, 12H), 1.22 (d, *J* = 6.9 Hz, 12H), 2.76 (sept, *J* = 6.9 Hz), 6.96–6.99 (m, 4H), 7.23–7.24 (m, 6H), 7.31 (s, 2H), 7.47 (t, *J* = 7.8 Hz, 2H), 7.53 (t, *J* = 7.7 Hz, 2H), 7.51–7.58 (m, 5H). ¹³C-NMR (CDCl₃, 100 MHz): 23.9 (qx4), 24.4 (qx4), 28.7 (dx4), 123.4 (dx2), 123.7 (dx2), 124.2 (dx4), 126.9 (dx2, appeared as a d, ²*J*_{C-P} = 9.4 Hz), 127.0 (s, appeared as a d, ¹*J*_{C-P} = 24.5 Hz), 130.2 (dx2, appeared as a d, ²*J*_{C-P} = 9.7 Hz), 130.5 (dx2), 132.7 (d), 135.8 (s), 137.4 (dx2), 137.7 (dx2, appeared as a d, ²*J*_{C-P} = 24.6 Hz), 145.7 (sx4), 150.0 (dx2, appeared as a d, ⁴*J*_{C-P} = 7.8 Hz), 159.6 (sx2, appeared as a d, ¹*J*_{C-P} = 5.1 Hz), 183.3 (s) ppm. IR (neat) ν 2962, 1581, 1446, 1328, 1102, 835, 752 cm^{−1}. HRMS (ESI): *m/z* calcd for C₄₃H₄₉N₄PCu [M-PF₆]⁺: 715.2991; found: 715.3011.

FULL PAPER

Computational details. Geometries were optimized with the B3LYP functional in which the DFT-D3 dispersion correction^[27] was included for a better description of long-range interactions such as CH- π interactions respectively between the dpa and NHC ligands. The effective core potential SDD was used for the copper atom and the 6-31+G(d,p) basis set for carbon, nitrogen, hydrogen, phosphor and oxygen atoms. Recently, we have shown that charge transfer states upon excitation play a crucial role in the photophysical properties of [Cu(NHC)(dpa)]⁺ complexes. Therefore, TD-DFT calculations were performed with the PBE0 functional that has been shown to be particularly relevant to describe TADF event.^[22] Both S₀-S₁ and S₀-T₁ transitions were considered and their natures were assigned plotting the Natural Transition Orbital analysis, in which molecular orbital contributions to a given transition are summed and weighted according to their CI coefficients. TADF were calculated from both optimized S₁ and T₁ energies. The former was calculated using the implemented TD-DFT gradients while the latter was obtained from open-spin-relaxed open shell calculations. Calculations were performed using the Gaussian 09 Revision D.01 package.^[28] Visualization were carried out with the VMD program.^[29]

Device preparation and analysis. Double layer LECs were fabricated as follows. ITO coated glass plates were patterned by conventional photolithography (Naranjo Substrates). The substrates were cleaned by using sequential ultrasonic baths, namely in water-soap, water, ethanol, and propan-2-ol solvents. After drying, the substrates were placed in a UV-ozone cleaner (Jetlight 42-220) for 8 min. An 100 nm layer of PEDOT:PSS was doctor-bladed onto the ITO-glass substrate to increase the device preparation yield (400 μ m substrate distance and a speed of 10 mm/s). The luminescent layer was entirely prepared with copper(I) complexes. The active layer was deposited by means of doctor blading technique (600 μ m substrate distance and a speed of 20 mm/s) reaching a thickness of 90-100 nm. These conditions resulted in homogenous thin films with a roughness less than 5 %, having no apparent optical defects. The latter was determined using the profilometer DektakXT from Bruker. Once the active layer was deposited, the samples were transferred into an inert atmosphere glovebox (<0.1 ppm O₂ and H₂O, Innovative Technology). Aluminum cathode electrode (90 nm) was thermally evaporated using a shadow mask under high vacuum (<1 x 10⁻⁶ mbar) using an Angstrom Covap evaporator integrated into the inert atmosphere glovebox. Time dependence of luminance, voltage, and current was measured by applying constant and/or pulsed voltage and current by monitoring the desired parameters simultaneously by using Avantes spectrophotometer (Avaspec-ULS2048L-USB2) in conjunction with a calibrated integrated sphere Avasphere 30-Irrad and Botest OLT OLED Lifetime-Test System. Electroluminescence spectra were recorded using the same spectrophotometer. Electrochemical impedance spectroscopic assays were carried out with a potentiostat/galvanostat (PGSTAT30, Autolab) equipped with a frequency response analyzer module (FRA). Measurements were performed at the applied voltage of 0 V after a LIV sweep from 0 to 7 V. The AC signal amplitude was set to 50 mV, modulated in a frequency range from 1 to 10⁶ Hz. The Nova 1.11 software was used to obtain the parameters from the R-R/C equivalent circuit.

Acknowledgements

This work was supported by the "Ministère de la Recherche et des Nouvelles Technologies", CNRS (Centre National de la Recherche Scientifique) and the LABEX SynOrg (ANR-11-LABX-0029). We thank the "Agence Nationale de la Recherche", within the CSOSG program (ANR-12-SECU-0002-02), the ANR program (ANR-15-CE39-0006) and the "Région Basse-Normandie" for their funding (F.S. and M.E.). M.L. acknowledges SeRC (Swedish e-Science Research Center) for funding. F.D.M. thanks the Swedish Research Council (Grant No. 621-2014-4646). F.D.M. and M.L. acknowledges SNIC (Swedish National Infrastructure for Computing) for providing computer resources (snic001-12-192). RDC and MDW acknowledge the support by

the 'Fonds der Chemischen Industrie' (FCI) in the Liebig grant framework. R.D.C. further acknowledges the program "Ayudas para la atracción de talento investigador – Modalidad 1 of the Consejería de Educación, Juventud y Deporte – Comunidad de Madrid with the reference number 2016-T1/IND-1463". F.D.M. and M.L. are grateful to Prof. J.C. Sancho-García for his generous support. SG thanks Johnson Matthey for the gift of metals.

Keywords: Copper(I) complexes • photoluminescence • Thermally activated delayed fluorescence • density functional theory • light-emitting electrochemical cell

- [1] a) R. D. Costa, E. Ortí, H. J. Bolink, F. Monti, G. Accorsi, N. Armaroli, *Angew. Chem. Int. Ed.* **2012**, *51*, 8178-8211. b) S. B. Meier, D. Tordera, A. Pertegás, C. Roldán-Carmona, E. Ortí and H. J. Bolink, *Mater. Today* **2014**, *17*, 217-223. c) Z. Yu, L. Li, H. Gao, Q. Pei, *Sci. China Chem.* **2013**, *56*, 1075-1086. d) E. Fresta, R. D. Costa, *J. Mater. Chem. C*, **2017**, *5*, 5643-5675.
- [2] a) Y.-M. Wong, F. Peng, Y.-B. Hou, Z. Xu, Y.-S. Wang, W.-F. Fu *Appl. Phys. Lett.* **2005**, *87*, 233512. b) N. Armaroli, G. Accorsi, M. Holler, O. Moudam, J.-F. Nierengarten, Z. Zhou, R. T. Wegh, R. Welter, *Adv. Mater.* **2006**, *18*, 1313-1316. c) R. D. Costa, D. Tordera, E. Ortí, H. J. Bolink, J. Schönle, S. Graber, C. E. Housecroft, E. C. Constable, J. A. Zampese, *J. Mater. Chem. C*, **2011**, *21*, 16108-16118. d) S. Keller, E. C. Constable, C. E. Housecroft, M. Neuburger, A. Prescimone, G. Longo, A. Pertegás, M. Sessolo, H. J. Bolink, *Dalton Trans.* **2014**, *43*, 16593-16593. e) C. Bizzarri, C. Strabler, J. Prock, B. Trettenbrein, M. Ruggenthaler, C.-H. Yang, F. Polo, A. Iordache, P. Brügge, L. D. de Cola *Inorg. Chem.* **2014**, *53*, 10944-10951. f) F. Brunner, L. Martinez-Sarti, S. Keller, A. Pertegás, A. Prescimone, E. C. Constable, H. J. Bolink, C. E. Housecroft, *Dalton Trans.* **2016**, *45*, 15180-15192. g) S. Keller, A. Pertegás, G. Longo, L. Martinez, J. Cerdá, J. M. Junquera-Hernández, A. Prescimone, E. C. Constable, C. E. Housecroft, E. Ortí, H. J. Bolink, *J. Mater. Chem. C* **2016**, *4*, 3857-3871.
- [3] a) D. Volz, M. Wallesch, C. Fléchon, M. Danz, A. Verma, J. M. Navarro, D. M. Zink, S. Bräse, T. Baumann *Green Chem.* **2015**, *17*, 1988-2011. b) E. Cariati, E. Lucenti, C. Botta, U. Giovannella, D. Marinotto, S. Righetto *Coord. Chem. Rev.* **2016**, *306*, 556-614.
- [4] a) H. Uoyama, K. Goushi, K. Shizu, H. Nomura, C. Adachi, *Nature* **2012**, *492*, 234-238. b) Y. Tao, K. Yuan, P. Xu, H. Li, R. Chen, C. Zheng, L. Zhang, W. Huang, *Adv. Mater.* **2014**, *26*, 7931-7958. c) R. Czerwieniec, M. J. Leidl, H. H. H. Homeir, H. Yersin, *Coord. Chem. Rev.* **2016**, *325*, 2-28. d) L. Bergmann, G. J. Hedley, T. Baumann, S. Bräse, I. D. W. Samuel, *Science Adv.* **2016**, *2*, e1500889.
- [5] G. Blasse, D. R. McMillin, *Chem. Phys. Lett.* **1980**, *70*, 1-3.
- [6] a) D. R. McMillin, K. M. McNett, *Chem. Rev.* **1998**, *98*, 1201-1220. b) C. T. Cunningham, J. J. Moore, K. L. H. Cunningham, P. E. Fanwick, D. R. McMillin, *Inorg. Chem.* **2000**, *39*, 3638-3644. c) M. Iwamura, S. Takeuchi, T. Tahara, *Acc. Chem. Res.* **2015**, *48*, 782-791. d) M. W. Mara, K. A. Fransted, L. X. Chen, *Coord. Chem. Rev.* **2015**, *282*, 2-18.
- [7] A. Kaeser, M. Mohankumar, J. Mohanraj, F. Monti, M. Holler, J.-J. Cid, O. Moudam, I. Nierengarten, L. Karmazin-Brelot, C. Duhayon, B. Delavaux-Nicot, N. Armaroli, J.-F. Nierengarten *Inorg. Chem.* **2013**, *52*, 12140-12151.
- [8] T. Gneuß, M. J. Leidl, L. H. Finger, H. Yersin, J. Sundermeyer, *Dalton Trans.* **2015**, *44*, 20045-20055.

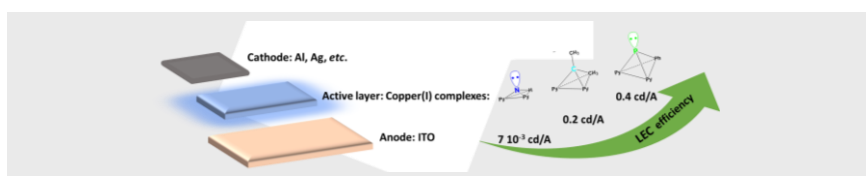
FULL PAPER

- [9] Z.-C. Fu, Q. Yin, Z.-F. Yao, C. Li, W.-F. Fu *J. Coord. Chem.* **2015**, *68*, 3282-3294.
- [10] J.-L. Chen, Z.-H. Guo, H.-G. Yu, L.-H. He, S.-J. Liu, H.-R. Wen, J.-Y. Wang *Dalton Trans.* **2016**, *45*, 696-705.
- [11] R. Visbal, M. C. Gimeno, *Chem. Soc. Rev.* **2014**, *43*, 3551-3574.
- [12] a) K. Matsumoto, N. Matsumoto, A. Ishii, T. Tsukuda, M. Hasegawa, T. Tsubomura *Dalton Trans.*, **2009**, 6795-6801. b) V. A. Krylova, P. I. Djurovich, M. T. Whited, M. E. Thompson, *Chem. Commun.* **2010**, *46*, 6696-6698. c) V. J. Catalano, L. B. Munro, C. E. Strasser, A. F. Samin *Inorg. Chem.* **2011**, *50*, 8466-8476. d) V. A. Krylova, P. I. Djurovich, J. W. Aronson, R. Haiges, M. T. Whited, M. E. Thompson, *Organometallics* **2012**, *31*, 7983-7993. d) P. Ai, M. Mauro, L. De Cola, A. A. Danopoulos, P. Braunstein *Angew. Chem., Int. Ed.* **2015**, *55*, 3338-3341. e) Z. Wang, C. Zheng, W. Wang, C. Xu, B. Ji, X. Zhang *Inorg. Chem.* **2016**, *55*, 2157-2164. f) R. Molteni, K. Edkins, M. Haenel, A. Steffen *Organometallics*, **2016**, *35*, 629-640. g) M. Nishikawa, T. Sano, M. Washimi, K. Takao, T. Tsubomura *Dalton Trans.* **2016**, *45*, 12127-12136. h) S. Shi, L. R. Collins, M. F. Mahon, P. I. Djurovich, M. E. Thompson, M. K. Whittlesey *Dalton Trans.* **2017**, DOI: 10.1039/C6DT04016K.
- [13] a) R. Marion, F. Sguerra, F. Di Meo, E. Sauvageot, J.-F. Lohier, R. Daniellou, J.-L. Renaud, M. Linares, M. Hamel, S. Gaillard, *Inorg. Chem.* **2014**, *53*, 9181-9191. b) R. Marion, F. Sguerra, F. Di Meo, E. Sauvageot, J.-F. Lohier, R. Daniellou, J.-L. Renaud, M. Linares, M. Hamel, S. Gaillard, *Inorg. Chem.* **2016**, *55*, 4068. c) M. Elie, F. Sguerra, F. Di Meo, M.; D. Weber, R. Marion, A. Grimault, J.-F. Lohier, A. Stallivieri, A. Brosseau, R. B. Pansu, J.-L. Renaud, M. Linares, M. Hamel, R. D. Costa, S. Gaillard, *ACS Appl. Mater. Interfaces* **2016**, *8*, 14678-14671.
- [14] a) V. A. Krylova, P. I. Djurovich, B. L. Conley, R. Haiges, M. T. Whited, T. J. Williams, M. E. Thompson, *Chem. Commun.* **2014**, *50*, 7176-7179. b) M. J. Leitzl, V. A. Krylova, P. I. Djurovich, M. E. Thompson, H. Yersin, *J. Am. Chem. Soc.* **2014**, *136*, 16032-16038.
- [15] T. L. Davis, J. L. Watts, K. J. Brown, J. S. Hewage, A. R. Treleven, S. V. Lindeman, J. R. Gardinier, *Dalton Trans.* **2015**, *44*, 15408-15412.
- [16] G. Dyker, O. Muth, *Eur. J. Org. Chem.* **2004**, 4319-4322.
- [17] N. Vedernikov, R. Miftakhov, S. V. Borisoglebski, K. G. Caulton, B. N. Solomonov, *Chem. Heterocyclic Comp.* **2002**, *38*, 406-416.
- [18] S. A. Saucedo Anaya, A. Hagenbach, U. Abram, *Polyhedron* **2008**, *27*, 3587-3592.
- [19] a) A. Kobayashi, T. Hasegawa, M. Yoshida, M. Kato *Inorg. Chem.* **2016**, *55*, 1978-1985. b) S. Hanf, R. Garcia-Rodriguez, S. Feldmann, A. D. Bond, E. Hey-Hawkins, D. S. Wright *Dalton Trans.* **2017** DOI: 10.1039/c6dt04390a.
- [20] M. E. Jung, G. Piizzi, *Chem. Rev.* **2005**, *105*, 1735-1766.
- [21] J. Nitsch, F. Iacemon, A. Lorbach, A. Eichhorn, F. Cisnetti, A. Steffen *Chem. Commun.* **2016**, *52*, 2932-2935.
- [22] M. Moral, L. Muccioli, W.-J. Son, Y. Olivier, J.-C. Sancho-García *J. Chem. Theory Comput.* **2015**, *11*, 168-177.
- [23] J. Föller, M. Kleinschmidt, C. M. Marian *Inorg. Chem.* **2016**, *55*, 7508-7516.
- [24] a) B. M. D. Puscher, M. F. Aygüler, P. Docampo, R. D. Costa, *Adv. Energy Mater.* **2017** DOI: 10.1002/aenm.201602283. b) M. D. Weber, J. E. Wittmann, A. Burger, O. B. Malcioğlu, J. Segarra-Martí, A. Hirsch, P. B. Coto, M. Bockstedte, R. D. Costa, *Adv. Funct. Mater.* **2016**, *26*, 6737-6750. c) L. D. Bastatas, K.-Y. Lin, M. D. Moore, K. J. Suhr, M. H. Bowler, Y. Shen, B. J. Holliday, J. D. Slinker, *Langmuir* **2016**, *32*, 9468-9474. c) A. Munar, A. Sandström, S. Tang, L. Edman, *Adv. Funct. Mater.* **2012**, *22*, 1511-1517.
- [25] C. A. Citadelle, E. Le Nouy, F. Bisaro, A. M. Z. Slawin, C. S. J. Cazin, *Dalton Trans.*, **2010**, *39*, 4489-4491.
- [26] G. C. Fortman, A. M. Z. Slawin, S. P. *Organometallics*, **2010**, *29*, 3966-3972.
- [27] a) S. Grimme, J. Antony, S. Ehrlich, H. Krieg *J. Chem. Phys.*, **2010**, *132*, 154104. b) S. Grimme, S. Ehrlich, L. Goerigk *J. Comput. Chem.* **2011**, *32*, 1456-1465.
- [28] M. J. Frisch, G. W. Trucks, H. B. Schlegel, G. E. Scuseria, M. A. Robb, J. R. Cheeseman, G. Scalmani, V. Barone, G. A. Petersson, H. Nakatsuji, X. Li, M. Caricato, A. Marenich, J. Bloino, B. G. Janesko, R. Gomperts, B. Mennucci, H. P. Hratchian, J. V. Ortiz, A. F. Izmaylov, J. L. Sonnenberg, D. Williams-Young, F. Ding, F. Lipparini, F. Egidi, J. Goings, B. Peng, A. Petrone, T. Henderson, D. Ranasinghe, V. G. Zakrzewski, J. Gao, N. Rega, G. Zheng, W. Liang, M. Hada, M. Ehara, K. Toyota, R. Fukuda, J. Hasegawa, M. Ishida, T. Nakajima, Y. Honda, O. Kitao, H. Nakai, T. Vreven, K. Throssell, J. A. Montgomery, Jr., J. E. Peralta, F. Ogliaro, M. Bearpark, J. J. Heyd, E. Brothers, K. N. Kudin, V. N. Staroverov, T. Keith, R. Kobayashi, J. Normand, K. Raghavachari, A. Rendell, J. C. Burant, S. S. Iyengar, J. Tomasi, M. Cossi, J. M. Millam, M. Klene, C. Adamo, R. Cammi, J. W. Ochterski, R. L. Martin, K. Morokuma, O. Farkas, J. B. Foresman, D. J. Fox *Gaussian 09*, Revision D.02, Gaussian, Inc., Wallingford CT, 2016.
- [29] W. Humphrey, A. Dalke, K. Schulten, *J. Mol. Graphics* **1996**, *14*, 33-38.

FULL PAPER

Entry for the Table of Contents

FULL PAPER



M. Elie, M. D. Weber, F. Di Meo, F. Sguerra, J.-F. Lohier, R. B. Pansu, J.-L. Renaud, M. Hamel, M. Linares, * R. D. Costa, * S. Gaillard*

Page No. – Page No.

In this work, we report the structural and electronic features of bis-pyridyl ligands onto cationic copper(I) complexes of general formula $[\text{Cu}(\text{IPr})(\text{N}^+\text{N})][\text{PF}_6]$. This study led to novel guideline in the design of enhancing the photo- and electro-luminescence features of this emerging family of copper(I) complexes.

Role of the bridging group in bis-pyridyl ligands: Enhancing both photo- and electro-luminescent features of cationic (IPr)Cu complexes